ChemComm

Accepted Manuscript

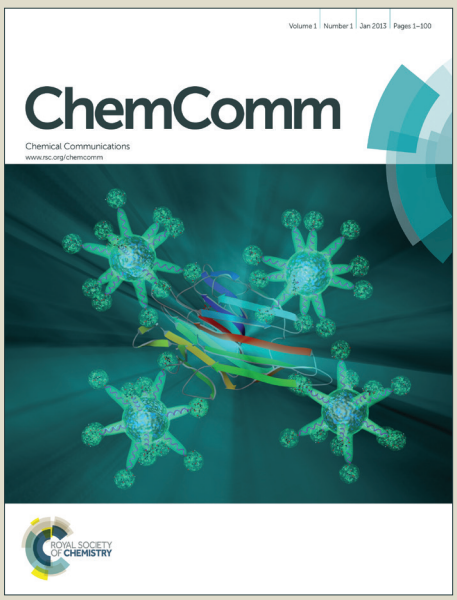

ROYAL SOCIETY OF CHEMISTRY

www.rsc.org/chemcomm

Journal Name

RSCPublishing

COMMUNICATION

Reformation of organic dicarboxylate electrode materials for rechargeable batteries by molecular self-assembly

Cite this: DOI: 10.1039/x0xx00000x

Received 00th January 2012,
Accepted 00th January 2012

DOI: 10.1039/x0xx00000x

www.rsc.org/

T. Yasuda[a] and N. Ogihara[a]

We have found that the specific capacity of a Li-intercalated metal-organic framework electrode material, 2,6-naphthalene dicarboxylate dilithium, can be increased by narrowing the distance between naphthalene layers via ordering. The increase in specific capacity can be attributed to formation of more efficient electron and ion pathways in the framework.

The operating potential of the anode is a critical factor for advanced rechargeable Li-ion batteries in large-scale applications because of the balance between energy density and safety. Operating conventional graphite anodes at a potential of 0.1 V (*vs.* Li/Li^+) poses a considerable risk to lithium metal deposition, which would provide an internal short circuit in a full cell.[1] As an alternative, transition metal oxide anodes, such as spinel lithium titanate ($Li_4Ti_5O_{12}$),[2] anatase, rutile-bronze (TiO_2-B),[3-6] and mesoporous MnO_2 nanosheets,[7] have been proposed, which can operate at potentials of 1.0–1.6 V. However, these anode materials significantly decrease the cell voltage; therefore, they must be used at an intermediate operating potential of 0.5–1.0 V as a good compromise providing high voltage as well as safety. In another approach, organic dicarboxylates have been used.[8-12] Since these materials can be operated at the target potential, we chose to examine an organic dicarboxylate: the intercalated metal–organic framework (iMOF)[13] (or coordination network, which means alkali metal–carboxylate based MOF),[14] 2,6-naphthalene dicarboxylate dilithium ($2,6\text{-Naph}(COOLi)_2$).[15, 16] As shown in Fig. 1(a), the proposed material has a characteristic organic–inorganic layered crystal structure composed of π-stacked naphthalene and tetrahedral LiO_4 network units, respectively, that form by molecular self-assembly. This material exhibits reversible Li intercalation with two electron transfers (220 mAh g^{-1}) at an operating potential of 0.7 V (*vs.* Li/Li^+).

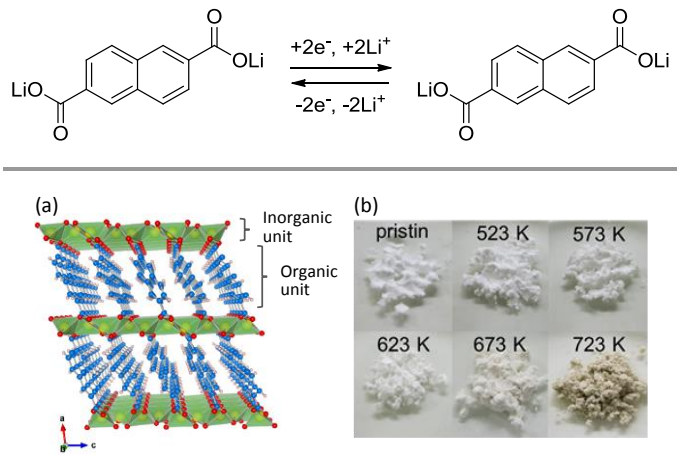

Fig. 1 (a) Crystal structure of 2,6-naphthalene dicarboxylate dilithium and (b) photograph of pristine and annealed samples.

Furthermore, due to no Li-Al alloy reactions at potentials over 0.4 V, the proposed anode material can have Al as the current collector, and high-voltage bipolar batteries can have Al current collectors for both the cathode and anode. We believe that the favorable electrochemical behavior of an ideal organic–inorganic layered crystal structure is related to efficient electron and lithium ion pathways. Banerjee *et al.* have reported preparation of a single crystal by refluxing for one week a solution of dicarboxylic acid and Li with Brönsted base in dimethylformamide solvent to effect ion exchange.[17] An ion-exchange reaction through freeze drying has also been reported by another research group.[18] In the latter method, many impurities in the layers were found,

as determined from X-ray diffraction patterns; these impurities limit electrochemical performance with respect to large initial irreversible capacity, reversible capacity, and cycle stability.

In this study, we systematically investigated the preparation of ideal crystals of 2,6-Naph(COOLi)$_2$ by controlling the molecular self-assembly using heat treatment. The 2,6-Naph(COOLi)$_2$ was synthesized by the ion-exchange reaction of 2,6-naphthalene dicarboxylic acid and LiOH·H$_2$O with refluxing under methanol followed by removal of the solvent. Since the proposed material shows high thermal stability at 800 K (527°C), as shown in Fig. S1, we annealed the sample powder at temperatures between 523 and 723 K for 12 h under an Ar atmosphere. As shown in Fig. 1(b), the product was a white or gray powder with ~10 mm needle-shaped crystals (Fig. S2). No color change was observed in comparison with the pristine sample (non–heated sample) at annealing temperatures of 523–673 K. On the other hand, the color changed from white to grayish-white over 673 K.

All Li/2,6-Naph(COOLi)$_2$ cells showed a flat plateau at a potential of 0.7 V, which corresponds to Li intercalation reaction (Fig. S3), and electrochemical reversibility (Fig. S4). As shown in Fig. 2(a), the cell using the pristine sample had a sloped discharge profile for potentials < 0.7 V during discharge. This result implies that the pristine sample has various crystal structures, including impurities, which means partial disordering. On the other hand, none of the annealed samples exhibited such sloped discharge profiles. As shown in inset of Fig. 2(a), the discharge capacities of the annealed samples were ~20mAh g^{-1} more than that of the pristine sample; the sample annealed at 623 K had the highest specific capacity of 213 mAh g^{-1}, which is nearly the theoretical capacity. The samples annealed over 673 K had slightly lower specific capacities than the samples annealed under 623 K. Differential capacity *dQ/dV* plots were calculated to determine the polarization of the charge-discharge processes. As shown in Fig. 2(b) and (c), the samples annealed at 573-623 K had the highest Li intercalation potential (~0.805 V) at discharge process (Fig. 2(b)), whereas the samples annealed at 523 K had the lowest potential (~0.869 V) at charge process (Fig. 2(c)). The potential peak difference of the discharge and charge processes from the differential capacity *dQ/dV* plots decreased with increasing annealing temperature of up to 623 K. In contrast, the peak potential difference increased for samples annealed over 673 K. The potential peak difference suggest the polarization due to the internal resistance of the electrode active materials. Thus, this means that the annealing samples decreases the internal resistance for Li intercalation, with the lowest internal resistance for the samples annealed at 573 and 623 K. This trend is similar to the observed specific capacity with respect to annealing temperature. Therefore, the samples annealed at 573–623 K possesses a suitably high specific capacity as well as low internal resistance.

Figure 3 shows the dependence of the main X–ray diffraction patterns on annealing temperature for 2,6-Naph(COOLi)$_2$ for the (011) and (102) reflections, which correspond to the patterns of the inorganic tetrahedral LiO$_4$ network and the organic π-stacked naphthalene packing layers, respectively. The (011) reflection shifted very little with annealing; therefore, the structure of the tetrahedral LiO$_4$ network is not affected by annealing. On the other hand, with annealing, the (102) reflection shifted to higher peak angles with decreasing half width peak. For the pristine sample and sample annealed at 523 K, two peaks with high peak width were observed. This implies that several types of naphthalene packing and disordered structures exist for no or low-temperature annealing, consistent with the observed sloped discharge profile of the pristine sample (Fig. 2(a)). For annealing temperatures over 573 K, there is a single, narrow peak shifted positively, indicating ordering of the π-stacked naphthalene packing layers. These results suggest that annealing results in improving ordering of the naphthalene packing with no change in the tetrahedral LiO$_4$ network unit.

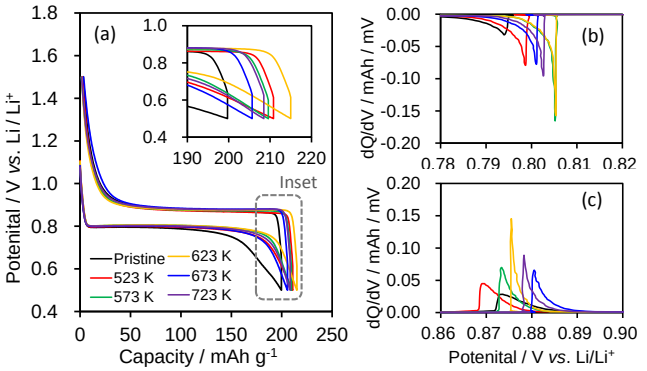

Fig. 2 Comparison of the (a) charge-discharge curves, inset: end of the discharge curves for a Li/2,6-Naph(COOLi)$_2$ cell using pristine 2,6-Naph(COOLi)$_2$ and samples annealed at various temperatures. Differential capacity *dQ/dV* plots of (b) the discharge and (c) charge processes, which were calculated from the data shown in Fig. 2(a).

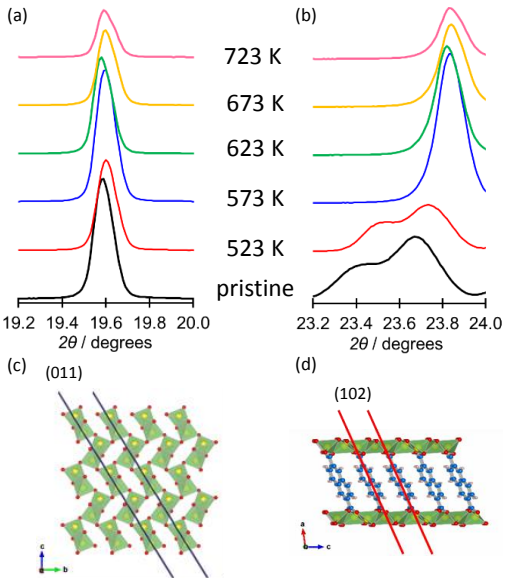

Fig. 3 Powder X-ray diffraction patterns for main reflections of (a) (011) and (b) (102) planes for pristine and annealed 2,6-Naph(COOLi)$_2$ samples, and schematic illustrations of (c) (011) plane of the inorganic unit of the tetrahedral LiO$_4$ network and (d) (102) plane of the organic unit of π-stacked naphthalene packing.

Using the Rietveld refinement method (Fig. S5), XRD patterns of samples annealed at temperatures over 573 K indicate a structure in good agreement with the reported structure for a single crystal.[14] The crystallographic data obtained from Rietveld refinement (Table S1) indicate that with increasing annealing temperature, the volume of the unit cell decreases and the density increases. Comparing specific capacity obtained from the charge-discharge tests and the lattice constant

of the unit cell, the specific capacity showed a correlation with changes in the *c*-axis. Figure 4 shows a comparison of the specific discharge capacity (Fig. 4(a)), IV resistance (Fig. 4(b)) and the length of the *c*-axis for annealed samples as a function of the annealing temperature. The specific capacity was highest for the sample annealed at 623 K, and slightly decreased with higher annealing temperatures. A similar trend was confirmed with respect to the IV resistance, which were calculated from the data of the polarization (V) obtained from the potential peak gap of the differential capacity *dQ/dV* plots shown in Fig. 2 (b) and (c) and the measured current (I). The IV resistance was lowest for the sample annealed at 573 K. On the other hand, the length of the *c*-axis decreases with increasing annealing temperature and remains relatively constant for annealing temperatures greater than 573 K. The *c*-axis corresponds to the (102) reflection, i.e., the direction of the π-stacked naphthalene packing, as shown in Fig. 3(d). This relationship indicates that the specific capacity increases and internal resistance decreases because of the formation of an efficient electron and ion pathway in the framework with narrowing of the π-stacked naphthalene interlayer distance through ordering by molecular self-assembly. For samples annealed at temperatures over 573 K, the samples become redox inert, partially because they begin to carbonize, as evidenced by the increase in the baseline at low angles of the XRD patterns (Fig. S5). In addition, the initial irreversible capacity (Fig. S4) of the samples annealed at temperature over 623 K become large. This may be due to the electrolyte decomposition at the product obtained.

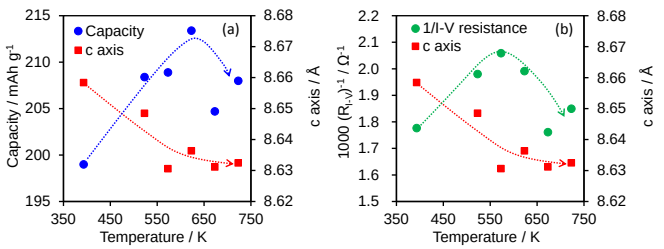

Fig. 4 (a) Changes in the specific capacities and *c*-axis as a function of annealing temperature. (b) Changes in the inverse of the calculated IV resistance and *c*-axis as a function of annealing temperature. The IV resistances were calculated from the data of the polarization (V) obtained from the potential peak gap of the differential capacity *dQ/dV* plots shown in Fig. 2 (b) and (c) and the measured current (I).

Conclusions

In conclusion, we systematically studied the correlation between electrochemical performance and ordering of the crystal structure for the intercalated metal-organic framework, 2,6-Naph(COOLi)$_2$, by controlling molecular self-assembly using annealing. We found that the dense π-stacked packing of the organic naphthalene moiety achieved through ordering was a key factor in improving electrochemical performance. The samples annealed at temperatures at 573–623 K had high specific discharge capacity and low internal resistance.

Acknowledgements

The authors acknowledge Prof. H. Uekusa of Tokyo Institute of Technology for powder XRD analysis and Dr. T. Sasaki of Toyota Central R&D Labs, Inc., for fruitful discussions.

Notes and references

[a]Toyota Central R&D Laboratories, Inc., Nagakute, Aichi, 480-1192, Japan. E-mail: ogihara@mosk.tytlabs.co.jp; Tel: +81-561-71-8127

† Electronic Supplementary Information (ESI) available: [details of any supplementary information available should be included here]. See DOI: 10.1039/c000000x/

1. I. Plitz, A. DuPasquier, F. Badway, J. Gural, N. Pereira, A. Gmitter and G. G. Amatucci, *Appl. Phys. A*, 2005, **82**, 615-626.
2. T. Ohzuku, A. Ueda and N. Yamamota, *J. Electrochem. Soc.*, 1995, **142**, 1431-1435.
3. A. R. Armstrong, G. Armstrong, J. Canales and P. G. Bruce, *Angew. Chem. Int. Ed. Engl.*, 2004, **43**, 2286-2288.
4. Z. Yang, D. Choi, S. Kerisit, K. M. Rosso, D. Wang, J. Zhang, G. Graff and J. Liu, *J. Power Sources*, 2009, **192**, 588-598.
5. J. Li, W. Wan, H. Zhou, J. Li and D. Xu, *Chem Commun (Camb)*, 2011, **47**, 3439-3441.
6. S. Liu, H. Jia, L. Han, J. Wang, P. Gao, D. Xu, J. Yang and S. Che, *Adv. Mater.*, 2012, **24**, 3201-3204.
7. M. Kundu, C. C. Ng, D. Y. Petrovykh and L. Liu, *Chem Commun (Camb)*, 2013, **49**, 8459-8461.
8. M. Armand, S. Grugeon, H. Vezin, S. Laruelle, P. Ribiere, P. Poizot and J. M. Tarascon, *Nat. Mater.*, 2009, **8**, 120-125.
9. W. Walker, S. Grugeon, H. Vezin, S. Laruelle, M. Armand, F. Wudl and J.-M. Tarascon, *J. Mater. Chem.*, 2011, **21**, 1615.
10. S. Wang, L. Wang, K. Zhang, Z. Zhu, Z. Tao and J. Chen, *Nano Lett.*, 2013, **13**, 4404-4409.
11. Y. Park, D. S. Shin, S. H. Woo, N. S. Choi, K. H. Shin, S. M. Oh, K. T. Lee and S. Y. Hong, *Adv. Mater.*, 2012, **24**, 3562-3567.
12. A. Abouimrane, W. Weng, H. Eltayeb, Y. Cui, J. Niklas, O. Poluektov and K. Amine, *Energy Environ. Sci.*, 2012, **5**, 9632-9638.
13. N. Ogihara, T. Yasuda, Y. Kishida, T. Ohsuna, K. Miyamoto and N. Ohba, *Angew. Chem. Int. Ed. Engl.*, 2014, 10.1002/anie.201405139R2.
14. D. Banerjee and J. B. Parise, *Crystal Growth & Design*, 2011, **11**, 4704-4720.
15. N. Ogihara, *JP2011-074054*, 2011.
16. N. Ogihara, *WO2012/053553*, 2012.
17. D. Banerjee, S. J. Kim and J. B. Parise, *Crystal Growth & Design*, 2009, **9**, 2500-2503.
18. L. Fedele, F. Sauvage, J. Bois, J. M. Tarascon and M. Becuwe, *J. Electrochem. Soc.*, 2013, **161**, A46-A52.